

AIM2 inflammasome is activated by pharmacological disruption of nuclear envelope integrity

Antonia Di Micco^{a,1}, Gianluca Frera^{a,1}, Jérôme Lugin^{a,1}, Yvan Jamilloux^{a,b}, Erh-Ting Hsu^c, Aubry Tardivel^a, Aude De Gassart^a, Léa Zaffalon^a, Bojan Bujisic^a, Stefanie Siegert^d, Manfredo Quadroni^e, Petr Broz^f, Thomas Henry^b, Christine A. Hrycyna^{c,g}, and Fabio Martinon^{a,2}

^aDepartment of Biochemistry, University of Lausanne, Epalinges 1066, Switzerland; ^bINSERM, U1111, Center for Infectiology Research, Lyon 69007, France; ^cDepartment of Chemistry, Purdue University, West Lafayette, IN 47907-2084; ^dFlow Cytometry Facility, Ludwig Center for Cancer Research, University of Lausanne, Epalinges 1066, Switzerland; ^eProtein Analysis Facility, Center for Integrative Genomics, University of Lausanne, Lausanne 1015, Switzerland; ^fFocal Area Infection Biology, Biozentrum, University of Basel, 4056 Basel, Switzerland; and ^gPurdue Center for Cancer Research, Purdue University, West Lafayette, IN 47907-2084

Edited by Zhijian J. Chen, University of Texas Southwestern Medical Center/Howard Hughes Medical Institute, Dallas, TX, and approved June 21, 2016 (received for review February 12, 2016)

Inflammasomes are critical sensors that convey cellular stress and pathogen presence to the immune system by activating inflammatory caspases and cytokines such as IL-1 β . The nature of endogenous stress signals that activate inflammasomes remains unclear. Here we show that an inhibitor of the HIV aspartyl protease, Nelfinavir, triggers inflammasome formation and elicits an IL-1R–dependent inflammation in mice. We found that Nelfinavir impaired the maturation of lamin A, a structural component of the nuclear envelope, thereby promoting the release of DNA in the cytosol. Moreover, deficiency of the cytosolic DNA-sensor AIM2 impaired Nelfinavir-mediated inflammasome activation. These findings identify a pharmacologic activator of inflammasome and demonstrate the role of AIM2 in detecting endogenous DNA release upon perturbation of nuclear envelope integrity.

inflammasome | nuclear envelope stress | DNA sensors | zmpste24 | Nelfinavir

Pattern-recognition receptors detect microbial components and danger signals released by damaged tissues to trigger inflammatory responses. Among these, members of the nucleotide-binding and oligomerization domain (NOD)-like receptors (NLRs) and AIM2-like receptors can assemble into enzymatically active complexes known as the inflammasomes (1). These complexes coordinate the recruitment and activation of inflammatory caspases to regulate the processing and release of bioactive cytokines including IL-1 β or IL-18 (2, 3). This pathway contributes to immune responses to pathogens, and its deregulation has been associated with inflammation in autoinflammatory syndromes as well as in complex diseases such as metabolic disorders and cancer (4, 5). In recent years tremendous progress has revealed several mechanisms involved in the activation of inflammasome (6).

Some inflammasome sensors have been shown to directly bind and recognize pathogen signatures. For example, the cytosolic release of microbial double-stranded DNA is detected by the C-terminal DNA-binding region of the protein AIM2. This leads to AIM2 oligomerization and the recruitment of the adaptor ASC and the protease caspase-1 to the forming inflammasome (7–10).

Other inflammasomes have been shown to detect intrinsic cellular perturbations. Potassium efflux, mitochondria dysfunction, and lysosomal disruption have been reported to mediate the activation of NLRP3, leading to the hypothesis that this inflammasome is a guardian of cellular integrity (11, 12). In addition to detecting mitochondrial perturbations, NLRP3 was found to be activated by endoplasmic reticulum (ER) stress in different tissues including macrophages (13, 14), liver (15), and insulin-producing β cells (16, 17). Inflammasome activation may therefore contribute to the low-grade inflammation (parainflammation) that characterizes stressed or malfunctioning cells, hence promoting adaptation and restoration of tissue function (18).

The HIV-protease inhibitors (HIV-PIs), in particular Nelfinavir (NFR), have been proposed to induce cellular stress both in vivo

and in vitro (19, 20). Beyond their broad use as anti-HIV drugs, these molecules display beneficial HIV-unrelated functions, anti-malaria, antituberculosis, and antitumor properties (20). At the cellular level, the HIV-PIs trigger an atypical ER stress-like transcriptional response that relies mostly on the activation of the integrated stress response (19, 21). However, the exact nature of the stress response engaged by these drugs is poorly understood, and its possible contribution to inflammation has not been investigated.

In brief, here we studied the stress response engaged by Nelfinavir and report that this molecule triggers robust inflammasome activation. Mechanistically, we found that Nelfinavir impaired the maturation of lamin A, a structural component of the nuclear envelope, thereby triggering a specific perturbation of cellular homeostasis here defined as “nuclear envelope stress.” We show that alterations of nuclear envelope integrity promote the release of DNA in the cytosol and consequent AIM2 activation. These findings demonstrate a function for AIM2 inflammasome in monitoring nuclear integrity by promoting activation of inflammatory caspases if cytosolic release of self-DNA is detected.

Results

The Antiviral Drug Nelfinavir Triggers the Release of IL-1 β to Promote Inflammation. Nelfinavir has been widely used in HIV-infected patients. Drug concentration can reach up to 17 μ M in the plasma

Significance

Inflammasomes are cellular sensors of harmful situations such as the presence of microbes or alterations in cellular homeostasis. Upon activation, inflammasomes trigger the proteolytic maturation and release of inflammatory cytokines to initiate immune and repair responses. The assembly of inflammasome relies on a diverse repertoire of sensor proteins that can detect specific stimuli. For example, the AIM2 inflammasome is activated by the presence of microbial DNA within the cytosol. In this paper, alterations of the nuclear envelope integrity are found to cause the exposure of nuclear DNA in the cytosol to promote the activation of the AIM2 inflammasome. Nuclear envelope stress can therefore directly engage innate immune sensors to elicit inflammation.

Author contributions: F.M. designed research; A.D.M., G.F., J.L., Y.J., E.-T.H., A.D.G., L.Z., B.B., and F.M. performed research; A.T., S.S., M.Q., P.B., T.H., and C.A.H. contributed new reagents/analytic tools; A.D.M., G.F., J.L., S.S., M.Q., C.A.H., and F.M. analyzed data; and F.M. wrote the paper.

The authors declare no conflict of interest.

This article is a PNAS Direct Submission.

Freely available online through the PNAS open access option.

¹A.D.M., G.F., and J.L. contributed equally to this work.

²To whom correspondence should be addressed. Email: fabio.martinon@unil.ch.

This article contains supporting information online at www.pnas.org/lookup/suppl/doi:10.1073/pnas.1602419113/-DCSupplemental.

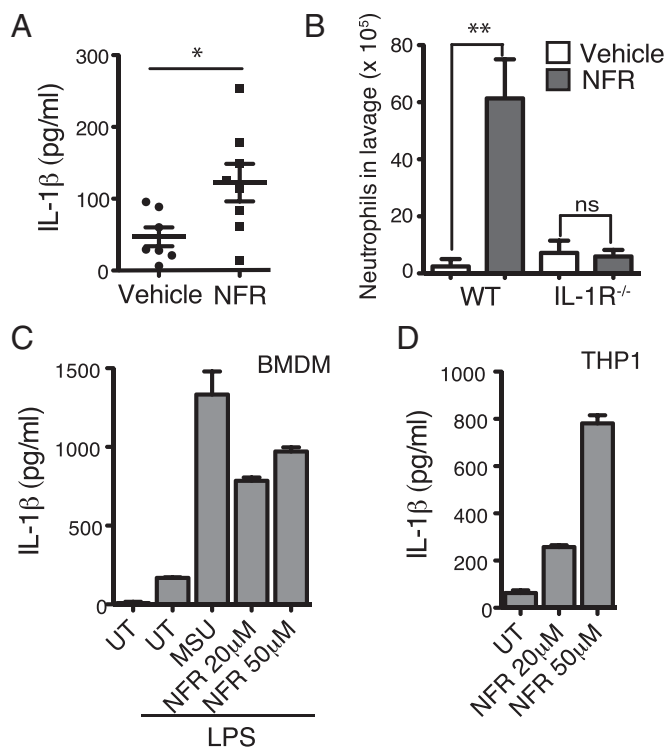


Fig. 1. NFR triggers the release of active IL-1 β . (A and B) Mice received intraperitoneally 0.2 mL of vehicle alone or supplemented with 100 mg/kg of NFR. Lavages were harvested after 5 h and analyzed for IL-1 β by ELISA (A). IL-1R^{+/+} (WT) and IL-1R^{-/-} were analyzed for neutrophil influx (CD11b⁺, LY6C⁺, LY6G⁺) by FACS (B). Data are pooled from two independent experiments and shown as means \pm SEM. * P < 0.05; ** P < 0.01 (six to eight mice per group were analyzed). (C) LPS-primed BMDMs were treated with MSU (positive control) and NFR as indicated. IL-1 β was monitored by ELISA at 6 h of treatment. Data are representative of at least three independent experiments. (D) PMA-differentiated THP-1 cells were stimulated with NFR for 6 h, and IL-1 β release was tested by ELISA. Data are representative of three independent experiments.

of treated patients (22, 23). We recently showed that concentrations can reach 10 μ M in liver tissues of mice treated with an i.p. dose of NFR reproducing the plasma concentration measured in patients (19). We used the same protocol to interrogate NFR-mediated inflammation in mice. Five hours after i.p. injection, NFR triggered the release of IL-1 β in the peritoneal lavage of treated mice (Fig. 1A). Consistent with these observations, NFR mediated a neutrophil influx that was impaired in IL-1R-deficient mice compared with control animals (Fig. 1B). These data indicate that NFR can mediate an IL-1-dependent peritonitis in mice similarly to well-known inflammasome activators (24). IL-1 β release by NFR was also observed in mouse bone marrow-derived macrophages (BMDMs) and differentiated THP-1 cells treated with NFR (Fig. 1C and D), indicating that NFR-mediated stress response may promote inflammation by directly inducing IL-1 β maturation and release.

Treatment with Nelfinavir Activates Caspase-1. Caspase-1 is the best-characterized protease triggering rapid proIL-1 β processing and maturation. To interrogate caspase-1 activation, we monitored its processing and release in the supernatant of immortalized BMDMs (iBMDMs). Upon treatment with NFR, caspase-1 processing was observed and correlated with released IL-1 β (Fig. 2A and B), suggesting that this protease may direct IL-1 β maturation in the context of NFR-mediated stress response. Investigation of a panel of HIV-protease inhibitors used in the clinic revealed

that most members of the family triggered some IL-1 β maturation and caspase-1 activation (Fig. S1A). However, we consistently found that, among these molecules, NFR is the most robust inducer of this pathway at relevant concentrations. In contrast, other anti-HIV drugs such as the nonnucleoside reverse transcriptase inhibitor Efavirenz did not trigger significant release of active IL-1 β (Fig. S1B).

Treatment of BMDMs with the pan-caspase inhibitor zVAD-FMK impaired NFR-mediated IL-1 β release (Fig. 2C). Similarly, caspase-1 and -11 deficiency dampened NFR-mediated IL-1 β release (Fig. 2D and Fig. S1C). Inflammatory caspase activation triggers pyroptosis, a type of cell death that correlates with the release of cytosolic content including cytokines and danger signals (25). We measured pyroptosis by monitoring LDH release and observed that NFR triggered a caspase-1/11-dependent form of

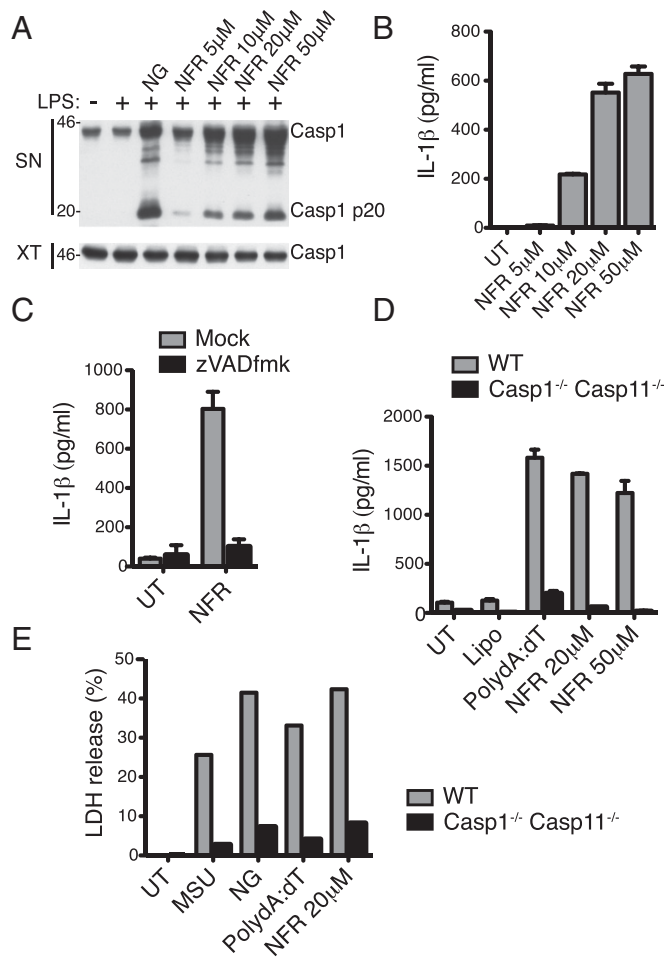


Fig. 2. Inflammatory caspases are required for IL-1 β release and pyroptosis upon treatment with NFR. (A–C) iBMDMs were primed with LPS and treated with 5 μ M NG for 1 h or NFR for 6 h at the indicated concentrations. Caspase-1 expression and maturation was probed by immunoblot in supernatant (SN) or cell extracts (XT) (A); released IL-1 β was measured by ELISA (B). The role of caspases was interrogated upon incubation with 20 μ M NFR in the presence or absence of zVAD-fmk (C). Data are representative of at least three independent experiments. (D) Released IL-1 β was measured by ELISA in LPS-primed caspase-1/11-deficient BMDMs or control cells (WT) treated for 6 h with Lipofectamine (Lipo), Lipo in combination with 1 μ g/mL poly(dA:dT) [Poly(dA:dT)], or NFR as indicated. Data are representative of three independent experiments. (E) LDH release from LPS-primed caspase-1/11-deficient BMDMs or control cells (WT) treated for 1 h with 5 μ M NG or 6 h with 50 μ g/mL MSU, 1 μ g/mL poly(dA:dT), or NFR as indicated. Data are representative of two independent experiments.

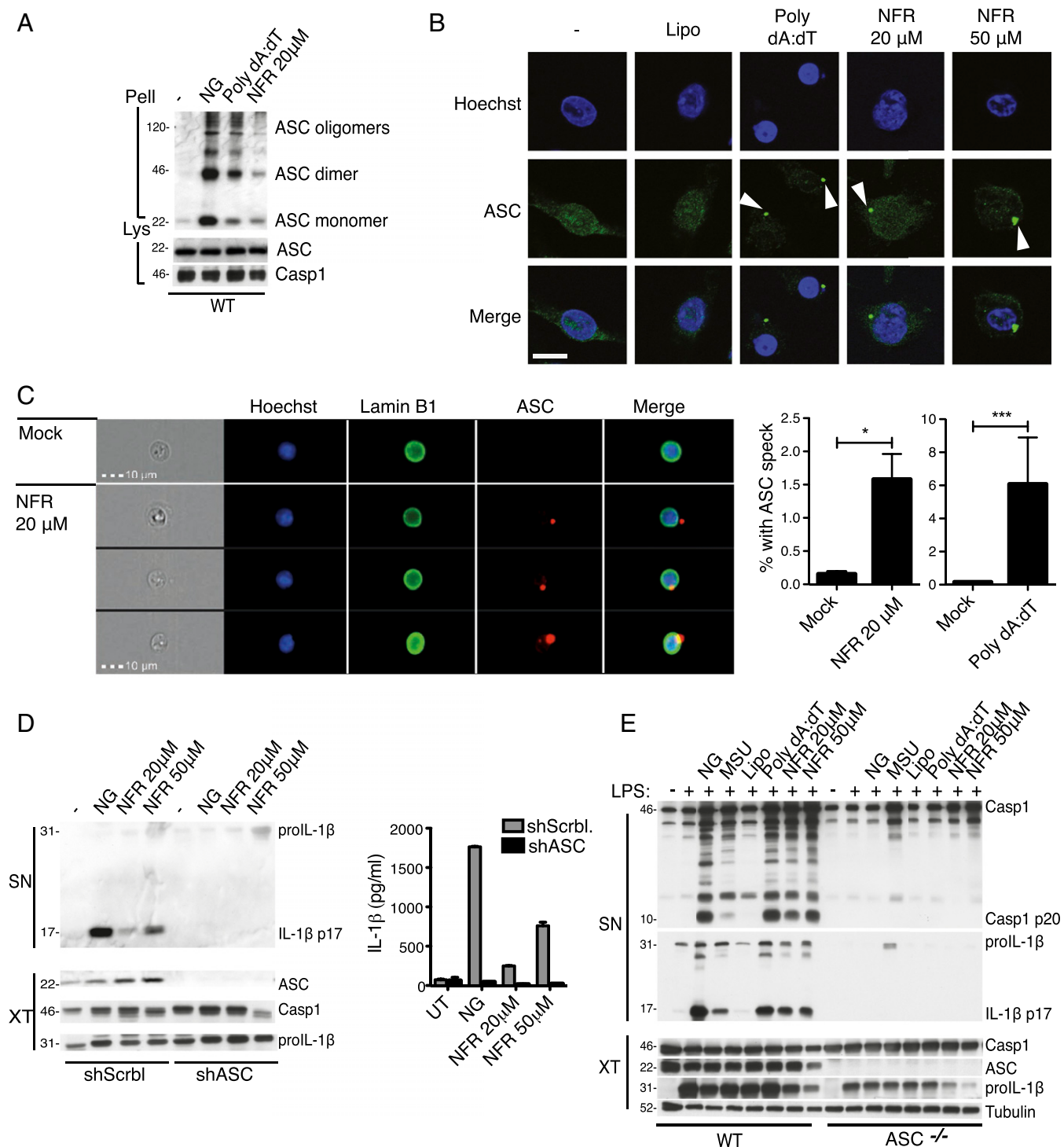


Fig. 3. NFR triggers the assembly of an ASC-dependent inflammasome. (A) BMDMs were primed with LPS and treated with NFR, poly(dA:dT), or NG as indicated. Cross-linked pellets (Pell) or soluble lysates (Lys) were immunoblotted for ASC or caspase-1. Data are representative of three independent experiments. (B) Immunofluorescence microscopy of BMDMs primed with LPS and treated with Lipo, Lipo in combination with 1 μ g/mL poly(dA:dT) [Poly(dA:dT)], or NFR as indicated. DNA staining is shown in blue (Hoechst); ASC staining is shown in green. Arrowheads indicate ASC inflammasome specks. (Scale bar: 10 μ m.) (C) ImageStream flow cytometric analysis of ASC inflammasomes. (Left) Representative images of LPS-primed BMDMs treated with vehicle (Mock) or NFR and stained with Hoechst in blue (DNA), lamin B1 in green (nucleus), and ASC in red. (Right) Quantification of ASC specks detected at 6 h upon treatment with poly(dA:dT) or NFR. Data are means \pm SEM from three independent experiments analyzing at least 20,000 cells. * P < 0.05; *** P < 0.001. (D) Human THP-1 macrophages expressing a scrambled shRNA (shScrbl) or an shRNA directed against ASC (shASC) were differentiated and primed with PMA (0.5 μ M) and treated with 5 μ M NG for 30 min or NFR for 6 h as indicated. (Left) Immunoblot of cleaved IL-1 β released in the supernatant (SN). Cell extracts were analyzed for ASC, caspase-1, and pro-IL-1 β expression. (Right) Secreted IL-1 β was measured by ELISA. (E) Immunoblot analysis of caspase-1 and IL-1 β maturation in ASC-deficient and control (WT) BMDMs primed with LPS as indicated and treated with NG, MSU, Lipo, poly(dA:dT), and NFR. SN: supernatants; XT: cell extracts. Tubulin was used as a loading control. Data are representative of three independent experiments.

cell death similar to other pyroptosis inducers such as monosodium urate (MSU), nigericin, or transfected poly(dA:dT) (Fig. 2E). Altogether these data suggest that treatment with NFR activates an inflammasome.

Nelfinavir Triggers the Formation of an ASC-Dependent Inflammasome.

The adaptor protein ASC is a major constituent of virtually all pyrin domain (PYD)-containing inflammasomes. Upon activation, ASC polymerizes and assembles into large ASC specks (26, 27). These aggregates can be detected biochemically by monitoring the precipitation of ASC in insoluble fractions and at the cellular level by confocal microscopy. Both approaches revealed endogenous ASC specks formation upon treatment of macrophages with NFR (Fig. 3A and B). To quantify inflammasome formation, we developed a protocol to detect ASC specks by imaging flow cytometry (Fig. 3C, Left). By gating on morphologically intact cells, we could quantitatively detect an inflammasome ASC speck in ~1.5% of NFR-treated cells and in 5% of cells transfected with poly(dA:dT) (Fig. 3C, Right). In both cases the measured enrichment was statistically significant, indicating that after a 6-h treatment a relatively small but significant number of live cells have visible inflammasome specks.

To demonstrate that ASC is essential for NFR-mediated inflammasome, we stably transfected THP-1 cells with a construct expressing a shRNA targeting human ASC. In this population IL-1 β maturation was decreased compared with cells expressing a control shRNA (Fig. 3D). Similarly, ASC deficiency abolished NFR-mediated inflammasome activity in mouse BMDMs (Fig. 3E and Fig. S2). Thus, the inflammasome activity observed upon treatment with NFR likely relies on a PYD-containing immune sensor.

NFR-Mediated Inflammasome Activation Is NLRP3-Independent. The NLRP3 inflammasome is a well-known sensor of cellular damage, ER stress, and metabolic stress (12, 28). However, compared with drugs that affect translation rates and trigger ER and integrated stress responses, we found that NFR is a more potent and rapid inducer of IL-1 β maturation (Fig. S3A). In line with these observations, NFR did not affect mitochondrial membrane potential, in contrast to NLRP3 activators and carbonyl cyanide *m*-chlorophenyl hydrazone (CCCP), a chemical inhibitor of oxidative phosphorylation (Fig. S3B). Moreover, NFR-mediated inflammasome activation was not significantly affected by NLRP3 deficiency (Fig. 4A). Inhibitors of NLRP3 activation, including the addition of extracellular potassium or antioxidants (29, 30), blocked inflammasome activity triggered by the NLRP3 activator nigericin, but did not affect NFR- or poly(dA:dT)-mediated caspase-1 activation (Fig. 4B). These findings indicate that NFR-mediated inflammasome assembly does not rely on typical NLRP3-activating pathways and may therefore define new mechanisms of inflammasome activation.

Nelfinavir Disrupts the Nuclear Envelope Integrity. The HIV-protease inhibitors were designed to target the active site of the HIV-protease. The observation that all of the inhibitors (except Amprenavir) activate the inflammasome (Fig. S1A) led us to hypothesize that these molecules may target a cellular protease. We used quantitative proteomics to search for putative cellular substrates, the processing of which could be impaired in the presence of NFR (31). To avoid cell death, we performed the experiment in HeLa as a model cell line that is not competent for inflammasome formation and subsequent pyroptosis. Cells treated with NFR or vehicle were analyzed by stable isotopic labeling with amino acids in cell culture (SILAC) coupled with protein molecular weight (MW) separation and mass spectrometry (Fig. 5A). This approach identified proteins displaying changes in electrophoretic mobility induced by NFR. Among the 19 putative candidates identified to have a pattern compatible with reduced processing,

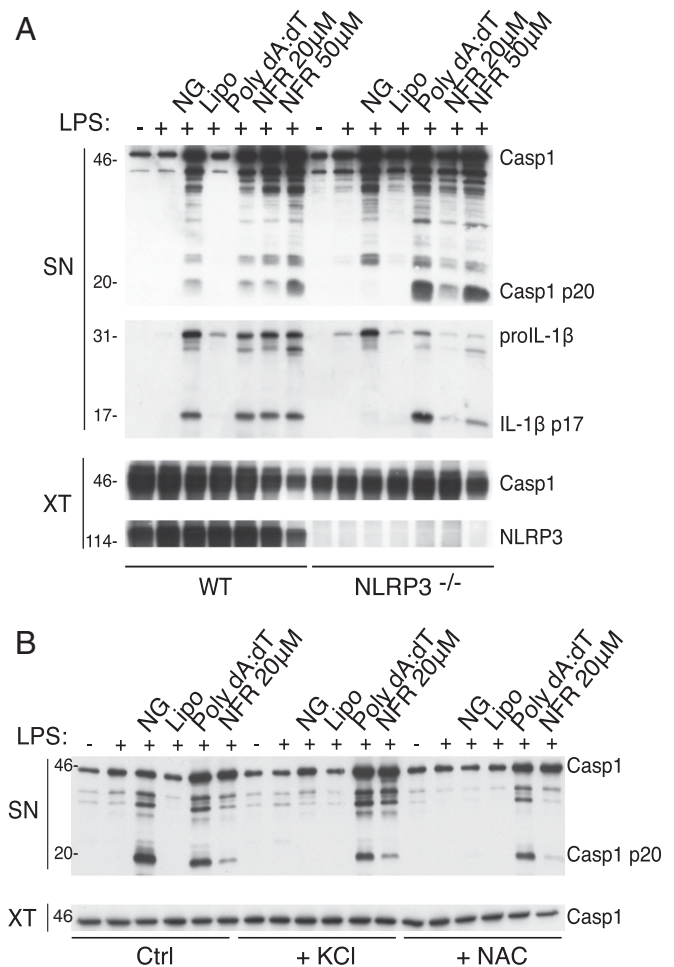


Fig. 4. Inflammasome activation is NLRP3-independent. (A) Immunoblot analysis of caspase-1 and IL-1 β maturation in NLRP3-deficient and control (WT) BMDMs primed with LPS as indicated and treated with NG for 30 min or with Lipo, poly(dA:dT), and NFR for 6 h. SN: supernatant; XT: cell extracts. Data are representative of at least three independent experiments. (B) LPS-primed iBMDMs were treated with Lipo, poly(dA:dT), or NFR for 6 h. These experiments were done in the absence or presence of 50 μ M KCl or 20 μ M of *N*-acetyl-cysteine (NAC). Caspase-1 activation and expression were measured by immunoblot of supernatant (SN) or cell extracts (XT), respectively. Data are representative of at least three independent experiments.

lamin A was selected as a promising target (Fig. S4). Lamin A is a component of the nuclear lamina, a scaffold structure underlying the inner nuclear membrane (32). The posttranslational maturation of lamin A is a highly regulated pathway that includes the proteolytic conversion of farnesylprelamin A to lamin A, a process that depends on the protease Zmpste24 (33). Zmpste24 deficiency and other mutations impairing the maturation of prelamins A to mature lamin A cause progeroid syndromes that include lipodystrophy as a typical feature (34). Similarly, treatments with HIV-PIs including NFR trigger lipodystrophy and metabolic deregulations in patients, which resemble syndromes caused by missense mutations in lamin A (35). The similarities between these symptoms has led to the observation that long-term treatments with some of the HIV-PIs, including Lopinavir, inhibit Zmpste24 activity and lamin A maturation (36), a finding that was not validated in peripheral blood mononuclear cells (37). In contrast, adipocytes differentiating in the presence of Indinavir or NFR showed altered lamin A maturation (38). In line with these observations, we found that, similar to the inhibitor of protein geranylgeranyltransferase (GGTI) that is a described antagonist of Zmpste24 (39), treatments with NFR triggered

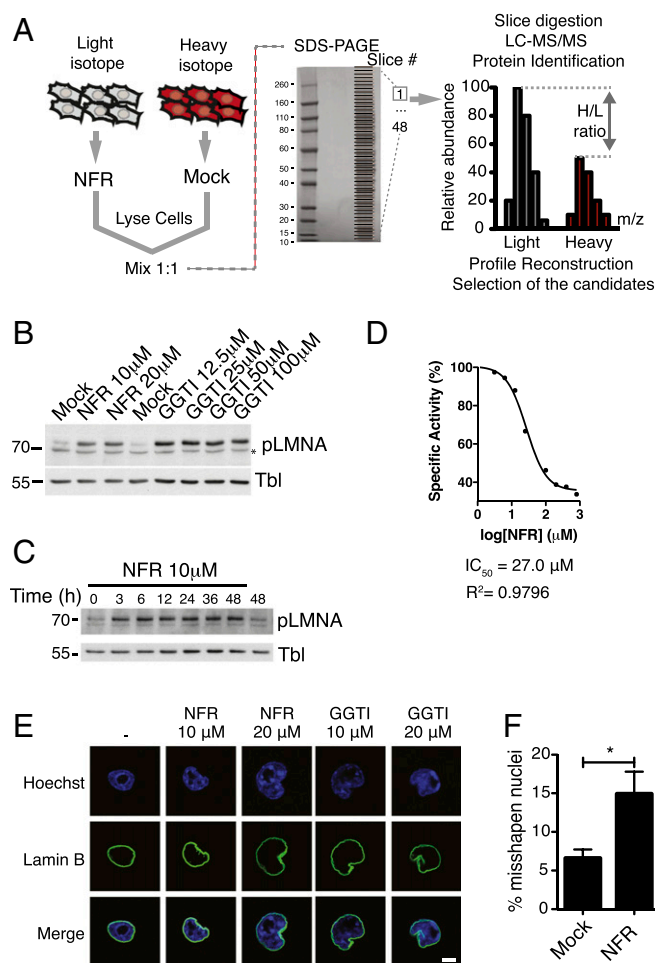


Fig. 5. Nelfinavir impairs lamin-A maturation. (A) Quantitative proteomics using SILAC. Two populations of HeLa cells were fully labeled with either normal (light) or heavy isotopes and treated with NFR or vehicle, respectively, for 6 h. After lysis and protein quantitation, the two samples were mixed at a 1:1 ratio, followed by gradient SDS/PAGE and cutting of the gel into 48 slices. Each gel slice was then submitted to trypsin digestion and LC-MS/MS and relative quantitation of proteins in each slice. The profiles along the gel are then reconstructed for each protein together with their abundance and heavy-over-light (H/L) ratios. Proteins with lower apparent molecular weight bands reduced and higher apparent molecular weight increased in the presence of NFR were considered candidate protease substrates affected by NFR. *m/z*, mass-to-charge ratio. (B and C) HeLa cells were treated with increasing doses of NFR or the Zmpste24 inhibitor GGTI for 6 h (B) or with 10 μM of NFR for the indicated times (C). Cell lysates were analyzed for prelamin A accumulation by immunoblotting. Tubulin (Tbl) was used as a loading control. Data are representative of at least three independent experiments. Asterisk indicates a nonspecific signal. (D) Inhibition of ZMPSTE24 by NFR as measured by the endoprotease-coupled methylation assay described in *Materials and Methods*. The assay was performed on membrane preparations from $\Delta ste24\Delta rce1$ yeast expressing human ZMPSTE24 using a synthetic farnesylated a-factor peptide as the substrate. The results are presented as percentage of the specific activity measured in presence of vehicle. Data are representative of three independent experiments. (E) Immunofluorescence microscopy of BMDMs treated 6 h with NFR or the Zmpste24 inhibitor GGTI as indicated. DNA staining is shown in blue (Hoechst); lamin B staining is shown in green. Representative images with misshapen nuclei are shown. (Scale bar: 10 μm.) (F) ImageStream flow cytometric analysis of nuclear shapes. Quantification of misshapen nuclei detected in BMDMs treated for 6 h with NFR or vehicle (Mock). Data are means ± SEM from three independent experiments analyzing at least 20,000 cells. **P* < 0.05.

the accumulation of prelamin A (Fig. 5B). Increased prelamin A accumulation was observed as early as 3 h after treatment with NFR (Fig. 5C), confirming that this molecule is a rapid and efficient

inhibitor of lamin A maturation. We performed a cycloheximide chase after GGTI washout. In this experiment GGTI washout restored the maturation of prelamin A in absence of de novo protein synthesis. When the washout was performed in presence of NFR, maturation of prelamin A was delayed and some prelamin A was detected 4 h after washout (Fig. S5A). These findings are consistent with previous reports (36, 38) and suggest that NFR may affect prelamin A maturation by inhibiting Zmpste24. Zmpste24 enzymatic activity can be measured with an endoprotease-coupled methylation assay using a synthetic farnesylated a-factor peptide substrate (40). In this assay, Zmpste24 cleaves the substrate, rendering it available for methylation isoprenylcysteine carboxyl methyltransferase. By measuring substrate methylation to quantify Zmpste24 activity, we found that NFR inhibited Zmpste24 in a dose-dependent manner (Fig. 5D) similarly to GGTI, ritonavir, and lopinavir (Fig. S5B). In contrast, Amprenavir did not inhibit Zmpste24 activity (Fig. S5B). Taken together, these data demonstrate that NFR can rapidly affect lamin A maturation to promote accumulation of prelamin A in cells.

As structural components, nuclear lamins provide morphological and mechanical stability to the nucleus. Defects in lamin A maturation have been associated with significant changes in nuclear shape (41). Consistently, NFR and GGTI were found to affect nuclear morphology both in BMDMs (Fig. 5E) and HeLa cells (Fig. S6A). This was quantified by imaging flow cytometry, confirming that NFR significantly increased the number of cells harboring a misshapen nucleus (Fig. 5F and Fig. S6B). This effect was not inhibited by the caspase inhibitor zVAD-fmk, indicating that alteration of nuclear shape was not a result of inflammasome-mediated caspase activation (Fig. S6C).

Nelfinavir Triggers the Release of Nuclear DNA. Mutations affecting lamin A maturation have been shown to cause nuclear envelope stress characterized by intermittent, nonlethal ruptures of the nuclear envelope, which can lead to temporary exchange of components between the nuclear and cytoplasmic compartments (42). Consistent with these observations, we found that treatment with NFR triggered the detection of DNA in the cytosol (Fig. 6A and Fig. S6D). We used imaging flow cytometry to quantify NFR-mediated DNA release. The analysis confirmed that NFR induced a significant DNA release in the cytosol (Fig. 6B). This DNA release was not accompanied with increased phosphorylation of γ H2AX or CHK1, indicating that NFR does not promote significant DNA damage (Fig. S7).

Given that the innate immune system samples the presence of double-stranded DNA in the cytosol as a marker of viral and bacterial infections, it is therefore conceivable that the release of self-DNA could engage innate immune sensors. For example, the protein cyclic GMP-AMP synthase (cGAS)-stimulator of interferon genes (STING) pathway detects the presence of cytosolic DNA and, in response, triggers expression of inflammatory mediators related to the type I IFN response (43). Treatment with NFR for 15 h triggered the expression of typical type I IFN-responsive genes such as *Cxcl10* and *Isg15* in cGAS-proficient BMDMs but not in cGAS-deficient BMDMs (Fig. 6C). Similarly, NFR-mediated induction of *Ifn β* , *Cxcl10*, and *Isg15* was cGAS-dependent in mouse embryonic fibroblasts (MEFs) (Fig. S8A). We performed genome editing by means of CRISPR/Cas9 to inactivate the *STING* gene in HeLa cells and confirmed that STING is required for NFR-mediated induction of *Isg15* in HeLa cells (Fig. S8B). Moreover, inactivation of *Zmpste24* by CRISPR/Cas9 in HeLa cells triggered basal increase in *Isg15* (Fig. S8C). These observations indicate that perturbation of lamin A maturation with NFR or by altering *Zmpste24* expression activates the DNA-sensing pathway cGAS-STING and support the finding that DNA is detected in the cytosol of NFR-treated cells.

In line with these observations, we found that overexpression of the cytosolic DNase TREX1 decreased inflammasome

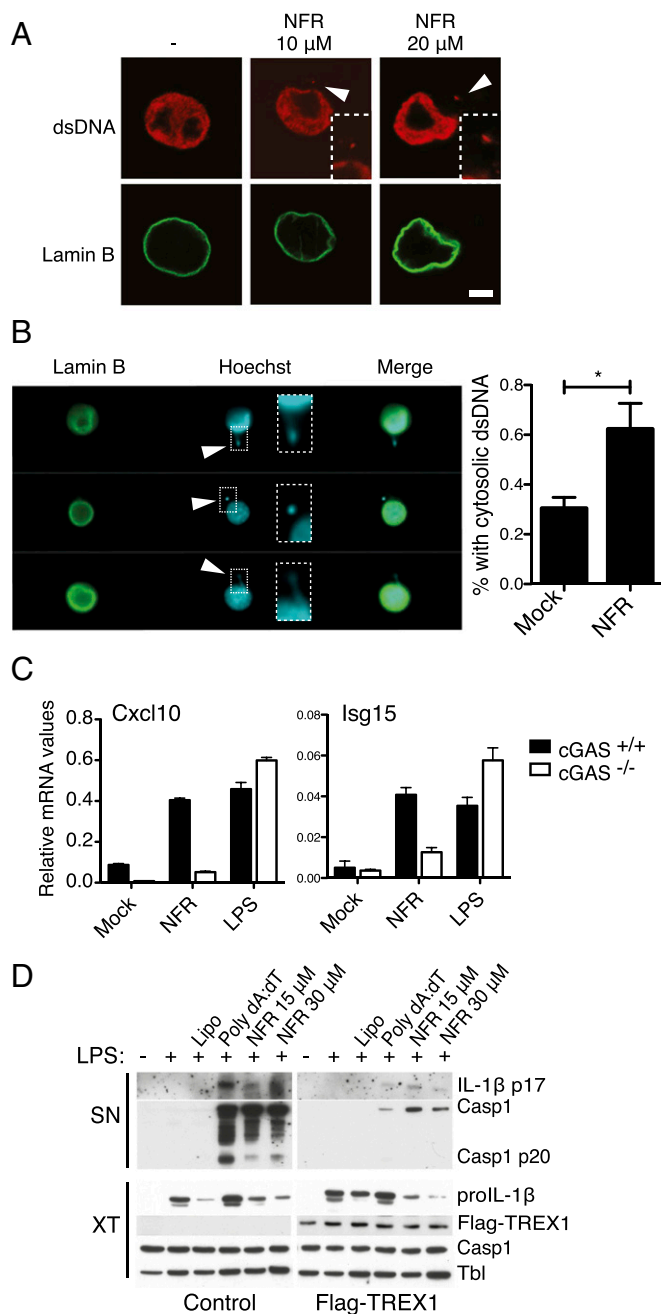


Fig. 6. Nelfinavir promotes the release of nuclear DNA. (A) Immunofluorescence microscopy of BMDMs treated for 6 h with NFR. Staining for dsDNA (red) and lamin B (green) is shown. Representative images with cytosolic dsDNA are shown. (Scale bar: 10 μ m.) (B) ImageStream flow cytometric analysis of cytosolic DNA content. (Upper) Representative images of extra nuclear DNA detected in the cytosol of BMDMs treated for 6 h with NFR. (Lower) Quantification of cells with cytosolic DNA. Data are means \pm SEM from three independent experiments analyzing at least 20,000 cells. * $P < 0.05$. (C) Relative mRNA levels measured by RT-qPCR of *Cxcl10* and *Isg15* in *cGas*^{+/+} and *cGas*^{-/-} BMDMs stimulated for 15 h with 25 μ M NFR or 500 ng/mL LPS. (D) iBMDMs stably overexpressing a Flag-tagged version of TREX1 or control population were primed with LPS as indicated and treated with Lipo, poly(dA:dT), and NFR. Caspase-1 and IL-1 β maturation were analyzed by immunoblotting. Tubulin (Tbl) is used as a loading control. SN: supernatant; XT: cell extracts. Data are representative of two independent experiments.

activation by NFR (Fig. 6D) but not by the NLRP3 activator Nigericin (Fig. S9), indicating that cytosolic release of DNA may act as a stress signal that promotes inflammasome assembly.

The AIM2 Inflammasome Is a Sensor of Cytosolic Self-DNA. Cytoplasmic transfection of poly(dA:dT), microbial, or host DNA has been shown to activate the AIM2 inflammasome (7–10). Reducing AIM2 expression by shRNA in THP-1 cells decreased NFR-mediated IL-1 β secretion, similar to the phenotype observed with the known AIM2 activator poly(dA:dT) (Fig. 7A). Likewise, AIM2-deficient BMDM and iBMDM clones impaired IL-1 β secretion in the presence of NFR (Fig. 7B and C). NFR-mediated caspase-1 processing was also impaired by AIM2 deficiency whereas MSU and nigericin response was unaffected (Fig. 7D). ASC oligomerization was also impaired in the absence of AIM2 (Fig. 7E), indicating that AIM2 is required for inflammasome assembly. Moreover, reconstitution of AIM2-deficient iBMDM with a construct expressing AIM2 restored poly(dA:dT) and NFR-mediated inflammasome activation (Fig. 7F), further demonstrating that AIM2 is key in sensing NFR-mediated stress response.

Treatment with the *Zmpste24* inhibitor GGTI triggered prelamins A accumulation leading to nuclear envelope defects and misshapen nuclei (39). We therefore tested whether this molecule activates an AIM2 inflammasome. Similarly to NFR, we found that GGTI triggered an IL-1 β secretion that is affected by AIM2 deficiency (Fig. 7G). AIM2 is therefore a key nuclear envelope integrity sensor that detects the release of self-DNA into the cytosol.

Discussion

The inflammasome was initially described as an ASC- and caspase-1-containing complex that spontaneously assembles in THP-1 cell extracts following disruption of cellular integrity using mechanical cell lysis in a hypotonic buffer (3). This led to the notion that, analogous to a model proposed in the field of plant immunity (44), some mammalian innate immune receptors may function as guardians of cellular integrity. Although NLRP3 has been described as a sensor of various cellular stresses, the detailed mechanisms of its activation are still a matter of debate, and very few intrinsic danger signals have been described.

Here we present several lines of evidence indicating that self-DNA can function as a relevant intrinsic signal leading to AIM2-dependent inflammasome activation: First, we demonstrate that NFR triggers the release of IL-1 β independently of the NLRP3 inflammasome. Second, we show that treatments with NFR reproduce a nuclear envelope stress response that causes the exposure of self-DNA in the cytosol. Third, we found that expression of the cytosolic DNA exonuclease TREX1 impairs inflammasome activation. And finally, we identified AIM2 as the inflammasome sensor that mediates IL-1 β release upon treatment with the *Zmpste24* inhibitor GGTI or NFR.

In transfection experiments AIM2 has been shown to detect dsDNA in a sequence-independent manner and from virtually any pathogen and species tested, including mammalian DNA (45–47). Evidence that AIM2 can recognize mammalian DNA is also supported by studies in inflammatory models. AIM2-dependent release of IL-1 β in the skin has been shown to contribute to the pathogenesis of psoriasis (48). In this disease, scavenging of DNA by the antimicrobial cathelicidin peptide LL-37 reduced IL-1 β secretion, suggesting that extracellular DNA (possibly of self-origin) could act as a danger signal. Similarly, in arthritis models driven by deficiency of the lysosomal endonuclease DNase2, the impaired ability of macrophages to degrade self-DNA released by damaged tissues triggers an inflammatory syndrome that is partially AIM2-dependent (49, 50).

Although these previous reports clearly suggest that self-DNA is a danger signal that can be released by dying cells (51), the notion that transient DNA exposure by stressed nuclear envelope structures can signal AIM2 activation is an intriguing notion that could have implications under different physiological and pathological conditions. Inside the body, cells are continuously

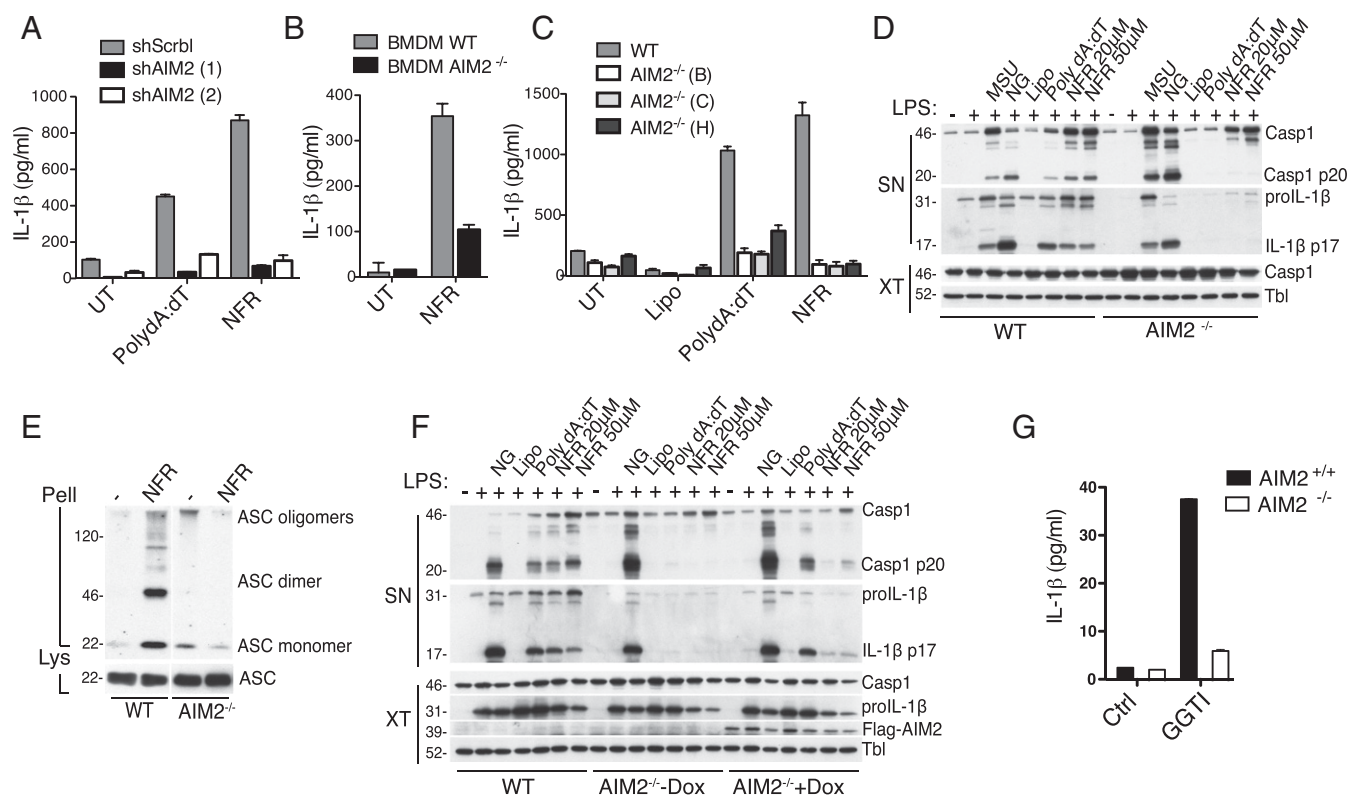


Fig. 7. The DNA-sensor AIM2 mediates NFR and GGT1-driven inflammasome activation. (A) Human THP-1 macrophages expressing a scrambled shRNA (shScrb1) or two independent shRNA directed against AIM2 (shAIM2) were differentiated and primed with PMA (0.5 μ M) and treated with poly(dA:dT) or NFR for 6 h as indicated. IL-1 β release was measured by ELISA. (B) LPS-primed BMDMs isolated from AIM2-deficient animals (AIM2^{-/-}) or controls (WT) were treated with 20 μ M NFR. IL-1 β release was measured by ELISA. (C) WT iBMDMs and three clones isolated from AIM2-deficient animals (clones B, C, and H) were primed with LPS and treated with Lipo, poly(dA:dT), or 20 μ M NFR for 6 h as indicated. IL-1 β release was measured by ELISA. (D) Immunoblot analysis of caspase-1 and IL-1 β maturation in AIM2-deficient and control (WT) BMDMs primed with LPS as indicated and treated with NG, MSU, Lipo, poly(dA:dT), and NFR. SN: supernatants; XT: cell extracts. Tubulin (Tbl) is used as a loading control. (E) iBMDMs from WT or AIM2-deficient mice were primed with LPS and treated with 20 μ M NFR. Cross-linked pellets (Pell) or soluble lysates (Lys) were immunoblotted for ASC. (F) Immunoblot analysis of caspase-1 and IL-1 β maturation in AIM2-deficient iBMDMs reconstituted with an inducible Flag-tagged AIM2 protein and control (WT) primed with LPS as indicated and treated with NG, Lipo, poly(dA:dT), or NFR. Doxycycline (Dox) was used to induce the AIM2 expression. SN: supernatants; XT: cell extracts. Tbl was used as a loading control. (G) LPS-primed iBMDMs from AIM2-deficient animals (AIM2^{-/-}) or controls (WT) were treated with 10 μ M of the Zmpste24 inhibitor GGT1, and IL-1 β release was measured by ELISA. Data in A–G are representative of at least three independent experiments.

exposed to physical forces and mechanical constraints of their microenvironment that can perturb membrane integrity. Oncogenic programs, infections, inherited mutations, and chemicals can increase these stresses and affect the ability of cells to cope with them (52, 53). For example, infection with HIV can cause dramatic nuclear envelope instability accompanied by prominent lamina gaps as well as large blebs of herniating chromatin resulting in the mixing of nuclear and cytoplasmic components (54). Because the human AIM2-like protein IFI16 was found to be activated by the cytosolic accumulation of incomplete HIV reverse transcripts to promote pyroptosis of lymphoid CD4 T cells (55), it would be interesting to interrogate the contribution of HIV-mediated nuclear envelope stress to pyroptosis. Inflammasome activation has also been detected in rhesus monkeys following mucosal simian immunodeficiency virus infection, both at the site of inoculation and at sites of distal virus spread (56), suggesting that this innate immune pathway may contribute to early defense against retroviruses. The fact that NFR can promote inflammasome activation raises the question of whether this drug may synergize with HIV to alter the course of infection in treated patients. Other innate immune sensors of cytosolic DNA engaged by treatment with NFR may also contribute to immunity against HIV, including cGAS, a pathway that has been shown to detect and drive inflammatory mediators upon infection with HIV (57).

Transient nuclear rupture has been observed in cultured laminopathy patient fibroblasts (42). Consistently, discontinuities of the nuclear envelope are visible by electron microscopy in hearts of mutant mice deleted for lysine 32 of lamin A (58) and in the liver of lamin A-deficient animals (59). Furthermore, in a mouse model of laminopathy caused by *Zmpste24*, an inflammatory phenotype was shown to contribute to aging (60). It is therefore tempting to speculate that the inflammasome could contribute to increased aging observed in laminopathies. Both pyroptosis and IL-1 secretion could contribute to chronic sterile parainflammation that characterizes aging in these diseases (61). Among the hallmarks of both laminopathies and treatments with the HIV-PIs, partial lipodystrophy is particularly remarkable (35). It is therefore likely that AIM2 activation in combination with other effects of nuclear membrane stress may contribute to these metabolic alterations (34).

Cancer cells also often exhibit changes in lamin A expression and nuclear morphology that resemble the phenotype observed in laminopathies, indicating that cancer cells may experience transient nuclear envelope rupturing (62, 63). This was shown experimentally; cancer cells forced to squeeze through tiny pores undergo repeated rupturing and repair of the nuclear envelope (64, 65), further indicating that the nuclear stress response is relevant to migrating cells, possibly contributing to metastasis. Interestingly, AIM2 expression is deregulated in various tumors,

and experiments in mice have shown that it has tumor suppressor properties; however, these effects may not rely on the assembly of a caspase-1-activating inflammasome (47, 66, 67). Whether nuclear rupture in cancer cells activates AIM2 to trigger pyroptosis and/or tumor immunogenicity is a tempting hypothesis that needs to be addressed. This hypothesis would be consistent with the observation that the ASC adaptor is down-regulated in many tumor types (68). Furthermore, in tumors expressing AIM2 and the other inflammasome components, NFR may synergize with preexisting nuclear envelope stress, possibly exacerbating cytosolic self-DNA exposure. This may contribute to the well-described NFR antitumoral properties (20).

The discovery that self-DNA can activate endogenous immune pathways raises an additional question that remains to be addressed. For example, it is unclear how AIM2 activation is prevented during mitosis. One possibility is that AIM2 is regulated by mitotic factors as reported for NLRP3 (69, 70). We previously showed that treatment with HIV-PIs triggers a transcriptional and translational reprogramming via the integrated stress response. Whether this pathway could contribute to nuclear envelope repair, similar to its role during endoplasmic reticulum stress response, is an open question that remains to be investigated.

In summary, our results identify AIM2 as a guardian of nuclear envelope integrity beyond its well-described role as a pathogen sensor and suggest that it may have regulatory functions in stressed tissues.

Materials and Methods

Cell culture, ELISA, chemicals and antibodies, generation of shRNA clones, generation of CRISPR/Cas9 clones, RNA extraction and RT-PCR of IFN-responsive genes, membrane potential measurement, and Slice-SILAC protein and MS analysis are described in *SI Materials and Methods*.

Isolation of BMDMs. Murine BMDMs were generated by crushing the femur and tibia bones from mice using a sterile mortar and pestle in 5 mL of DMEM, 2% (vol/vol) FBS, and 1% penicillin/streptomycin (P/S), and fluid was filtered with a nylon cell strainer. Cells were spun at $1,500 \times g$ for 10 min at 4 °C and plated in a 10-cm nonadherent petri dish. After 5 d the adherent cells were detached with 3 mL of accutase for 5 min and centrifuged at $1,500 \times g$ for 5 min. The cell pellet was resuspended and cultured in F12 medium (GIBCO), 20% (vol/vol) conditioned media from L929 cells, 10% (vol/vol) FBS, and 1% P/S.

Inflammasome Activation. Before stimulation, THP1 cells were differentiated for 3 h in the presence of 0.5 mM phorbol 12-myristate 13-acetate (PMA) (71). Cells were washed twice with PBS, plated onto 12-well plates, and left to adhere overnight. The following day, the culture medium was removed and replaced with fresh media before stimulation as indicated. BMDMs were plated in a 12-well plate overnight. The following day media were changed before stimulation with OPTIMEM (GIBCO) for the Western blot analysis or with complete RPMI media for the ELISA analysis. Cells were stimulated with 5 μ M of nigericin (NG) for 30 min; 5 mM of ATP for 1 h; and 10, 20, and 50 μ M of NFR for 6 h or 2 μ g of poly(dA:dT) was transfected for 3–4 h. After stimulation supernatant was collected and proteins were precipitated by the methanol/chloroform method.

Mice. Caspase-1^{-/-}, AIM2^{-/-}, NLRP3^{-/-}, ASC^{-/-}, and cGAS^{-/-} mice on a C57BL/6J background were previously described (24, 72, 73). Mice were bred in the Center of Infection and Immunity animal facility at the University of Lausanne or at the Plateau De Biologie Expérimentale De La Souris (Lyon, France). All animal experiments were approved by the Veterinary Office of the Canton de Vaud and the Animal Ethics Committee (authorization 2390) and were performed according to local guidelines.

Peritonitis Model. Peritonitis was induced in 7- to 12-wk-old age- and sex-matched mice by i.p. injection of 100 mg/kg of NFR. NFR was dissolved in delivery vehicle containing 10% (vol/vol) DMSO, 5% (vol/vol) PEG, and 5% (vol/vol) Tween 80. After 5 h the peritoneal cavity was flushed with sterile PBS. The lavage fluid was centrifuged, and the pelleted cells were counted and analyzed for the influx of neutrophils (CD11b+, LY6C+, LY6G+) by flow cytometry. Data were collected with a DB Accuri C6 flow cytometer (BD Biosciences) and analyzed with FLOWJO software.

Lactate Dehydrogenase Release Assay. Lactate dehydrogenase (LDH) is rapidly released into the cell-culture supernatant upon damage of the plasma membrane. The release of LDH was detected using the Cytotoxicity Detection kit from Roche. The kit was used according to the manufacturer's instruction.

Reconstitution of AIM2 KO Cells and Generation of TREX1-Overexpressing Cells. Lentiviral pINDUCER21 plasmid was obtained from Steve Elledge, Harvard Medical School, Boston (74). A human Flag-tagged AIM2 or TREX1 construct were cloned into the pENTR 1A dual selection vector (Invitrogen) and then cloned in the pINDUCER21, a GFP tet-inducible lentiviral vector plasmid. Lentiviruses were produced as previously described (75). AIM2^{-/-} iBMDMs were infected with AIM2-expressing lentiviruses, and iBMDM were infected with TREX1-expressing lentiviruses. GFP-positive cells were FACS-sorted 96 h postinfection. Cells were cultured in complete medium, and Flag-tagged AIM2 or TREX1 expression was induced using doxycycline (1 μ g/mL for 24 h).

ASC Oligomerization Assay. iBMDMs were primed with 100 ng of LPS for 3 h and then treated with 20 μ M NFR for 6 h and 5 μ M NG for 30 min or transfected with 2 μ g/mL poly(dA:dT) for 3–4 h. After stimulation the supernatant was kept to test IL-1 β release and caspase-1 cleavage by Western blot. Cells were detached with PBS containing 2 mM EDTA and centrifuged 5 min at $1,500 \times g$. Cells were lysed on ice in 500 μ L of Buffer A (20 mM Hepes-KOH, pH 7.5, 10 mM KCl, 1.5 mM MgCl₂, 1 mM EDTA, 1 mM EGTA, 320 mM sucrose) by syringing 30 times using a 21-G needle. The cell lysates were centrifuged in 1.5-mL Eppendorf tubes at $1,800 \times g$ for 8 min to remove the bulk nuclei, and 30 μ L of the supernatants were kept for Western blot analysis to test ASC expression in the lysates. The remaining supernatant was diluted two times with Buffer A and centrifuged 5 min at $2,000 \times g$. After centrifugation, supernatant was diluted with 1 vol of CHAPS buffer (20 mM Hepes-KOH, pH 7.5, 5 mM MgCl₂, 0.5 mM EGTA, 0.1 mM PMSF, 0.1% CHAPS) and again centrifuged at $5,000 \times g$ for 8 min to pellet the ASC pyroptosome. The supernatant was discarded and the pellet was resuspended in 50 μ L of CHAPS buffer with 4 mM of disuccinimidyl suberate (Thermo Scientific) for 30 min at room temperature (RT). Samples were centrifuged at $5,000 \times g$ for 8 min, and pellets were resuspended in 30 μ L of 2 \times loading buffer in nonreducing conditions for Western blot.

Endoprotease-Coupled Methylation Assays. The assays were performed as previously described with minor modifications (36, 39, 76). Reactions contained 5 μ g of membranes from *ste24 Δ rce1 Δ* yeast expressing human ZMPSTE24, 10 μ g of membranes expressing yeast isoprenylcysteine carboxyl methyltransferase Ste14p (77), 15 μ M farnesylated α -factor peptide [YIIKGVFWDPA-(Fr)CVIA] (EZ Biolabs), and 20 μ M S-adenosyl [¹⁴C-methyl]-L-methionine (55 mCi/mmol) (Perkin-Elmer) in 100 mM Tris-HCl, pH 7.5, in a final volume of 60 μ L. The reactions also contained HIV-PIs at the indicated concentration. After incubating the reactions at 30 °C for 30 min, the reactions were stopped with 50 μ L of 1 M NaOH/1% SDS and then spotted on pre-cut filter paper. Each filter paper was lodged into the neck of a vial containing 10 mL of scintillation fluid (RPI), capped, and allowed to diffuse at room temperature for 3 h. The base-releasable [¹⁴C]-methanol was quantified by liquid scintillation counting. Background counts from *ste24 Δ rce1 Δ* yeast with empty vector (77) were subtracted from each sample. IC₅₀ determinations were performed in triplicate and calculated by using GraphPad 4.0.

Immunofluorescence Staining for Image Stream Analysis. iBMDMs were seeded the day before the experiment in six-well plates and then stimulated for 4–6 h with the indicated concentrations of Nelfinavir, lipofectamine, or lipofectamine and 1 μ g/mL poly(dA:dT) in the presence of 1 μ g/mL LPS. Cells were detached and washed once with PBS containing 2 mM EDTA before fixation in fixation/permeabilization buffer [PBS, 2% (vol/vol) PFA, 0.3% Triton X-100] for 15 min at 4 °C. After two washes in FACS buffer [PBS, 2% (vol/vol) FCS, 0.3% Triton X-100, 2 mM EDTA], cells were incubated overnight at 4 °C with primary antibodies against ASC, dsDNA, and lamin B1 diluted 1:300 in FACS buffer. Cells were washed twice in FACS buffer and incubated for 1 h with secondary antibodies diluted 1:500 in FACS buffer at RT. Hoechst was added at a final concentration of 10 μ g/mL for the last 5 min of incubation with secondary antibodies. After a final wash, cells were resuspended in 50 μ L of FACS buffer and analyzed with the Image Stream.

Image Stream Analysis. Cells were acquired using Inspire software on a 4-laser 12-channel imaging flow cytometer Image StreamX MarkII (Millipore) using 40 \times magnification. At least 10,000 single cells were acquired per sample, with debris and doublets excluded based on their area and aspect ratio. For analysis, cells in focus (using the "gradient RMS" feature for the brightfield image) and single cells (in a plot using "area" versus "aspect ratio") were

gated. Based on the intensity, cells positively stained for lamin B, dsDNA, and ASC were selected, whereas cells with a sub-G0 DNA (based on Hoechst intensity) content were excluded. In addition, using a Hoechst threshold mask of 50% combined with the spot count feature, cells with fragmented nuclei that were presumable dead were excluded.

To assess the circularity of the nucleus, the circularity feature was calculated using morphology masks of lamin B and Hoechst, respectively. Cells showing circularity values higher than 10 for both features were considered to have round nuclei.

To analyze ASC speck formation, the area of the ASC signal was plotted against the Max pixel value of ASC. Signals with a small area and a high maximum pixel value were considered to be ASC specks. For analysis of dsDNA in the cytoplasm, a threshold mask of 80% for the dsDNA signal was calculated, which allowed to distinguish small dsDNA dots in the nucleus from the nucleus itself. Using the spot count feature on the dsDNA threshold mask, cells showing two or more dsDNA spots were considered to have dsDNA in the cytoplasm.

Immunofluorescence Staining for Confocal Microscopy. For confocal microscopy HeLa cells or iBMDMs were plated the day before the experiment on 15-mm coverslips in 12-well plates. After treatment the cells were fixed with 2% (vol/vol) PFA (Appllichem) for 20 min at RT. The cells were then permeabilized with 0.1% Triton X-100 in PBS for 10 min and washed once with PBS. The aspecific sites were blocked with 3% (wt/vol) BSA prepared in PBS for 30 min at RT. The antibodies against lamin B, dsDNA, and ASC were

diluted 1:500 in 1% BSA and incubated on the coverslips overnight at 4 °C. The next day the cells were washed five times with PBS, and the fluorescent secondary antibodies [anti-IgG(H+L) Alexa Fluor conjugates, Thermo Scientific] diluted 1:1,000 in 1% BSA were applied for 1 h. The coverslips were washed again with PBS and incubated 5 min with the Hoechst dye diluted in PBS at the final concentration of 4 µg/mL. The coverslips were mounted on slides using ProLong Gold Antifade (Invitrogen). Images were captured using an inverted confocal microscope LSM 510 META (Zeiss) equipped with a 63×/1.40 oil-immersion objective, processed with Zeiss Axiovision software, and analyzed with ImageJ across at least 10 fields from three independent experiments.

Statistical Analysis. All data are representative of at least three different experiments. Data are mean ± SEM of three independent experiments. For ImageStream analysis data comparing mock with NFR- or poly(dA:dT)-treated cells, *P* values were calculated using the two-sided Student *t* test, and three independent experiments with at least 20,000 cells per experiments were analyzed. For in vivo experiments, *P* values were calculated using the two-sided Student *t* test comparing NFR with vehicle.

ACKNOWLEDGMENTS. We thank S. Elledge, Andrea Ablasser, and the NIH AIDS Reagent Program for sharing key reagents; Denarda Dangaj, Andrea Ablasser, Ramanjaneyulu Allam, and Kendle M. Maslowski for comments and discussions; and the staff of the Lausanne Proteomic Facility for the Slice-SILAC experiments. This project is supported by European Research Council Starting Grant 281996.

- Wen H, Miao EA, Ting JP (2013) Mechanisms of NOD-like receptor-associated inflammasome activation. *Immunity* 39(3):432–441.
- Man SM, Kanneganti TD (2016) Converging roles of caspases in inflammasome activation, cell death and innate immunity. *Nat Rev Immunol* 16(1):7–21.
- Martinon F, Burns K, Tschopp J (2002) The inflammasome: A molecular platform triggering activation of inflammatory caspases and processing of proIL-β. *Mol Cell* 10(2):417–426.
- Guo H, Callaway JB, Ting JP (2015) Inflammasomes: Mechanism of action, role in disease, and therapeutics. *Nat Med* 21(7):677–687.
- Lamkanfi M, Dixit VM (2014) Mechanisms and functions of inflammasomes. *Cell* 157(5):1013–1022.
- Vanaja SK, Rathinam VA, Fitzgerald KA (2015) Mechanisms of inflammasome activation: Recent advances and novel insights. *Trends Cell Biol* 25(5):308–315.
- Fernandes-Alnemri T, Yu JW, Datta P, Wu J, Alnemri ES (2009) AIM2 activates the inflammasome and cell death in response to cytoplasmic DNA. *Nature* 458(7237):509–513.
- Hornung V, et al. (2009) AIM2 recognizes cytosolic dsDNA and forms a caspase-1-activating inflammasome with ASC. *Nature* 458(7237):514–518.
- Bürckstümmer T, et al. (2009) An orthogonal proteomic-genomic screen identifies AIM2 as a cytoplasmic DNA sensor for the inflammasome. *Nat Immunol* 10(3):266–272.
- Roberts TL, et al. (2009) HIN-200 proteins regulate caspase activation in response to foreign cytoplasmic DNA. *Science* 323(5917):1057–1060.
- Gurung P, Lukens JR, Kanneganti TD (2015) Mitochondria: Diversity in the regulation of the NLRP3 inflammasome. *Trends Mol Med* 21(3):193–201.
- Leemans JC, Cassel SL, Sutterwala FS (2011) Sensing damage by the NLRP3 inflammasome. *Immunol Rev* 243(1):152–162.
- Bronner DN, et al. (2015) Endoplasmic reticulum stress activates the inflammasome via NLRP3- and caspase-2-driven mitochondrial damage. *Immunity* 43(3):451–462.
- Menu P, et al. (2012) ER stress activates the NLRP3 inflammasome via an UPR-independent pathway. *Cell Death Dis* 3:e261.
- Lebeaupin C, et al. (2015) ER stress induces NLRP3 inflammasome activation and hepatocyte death. *Cell Death Dis* 6:e1879.
- Lerner AG, et al. (2012) IRE1α induces thioredoxin-interacting protein to activate the NLRP3 inflammasome and promote programmed cell death under irremediable ER stress. *Cell Metab* 16(2):250–264.
- Osowski CM, et al. (2012) Thioredoxin-interacting protein mediates ER stress-induced β cell death through initiation of the inflammasome. *Cell Metab* 16(2):265–273.
- Medzhitov R (2008) Origin and physiological roles of inflammation. *Nature* 454(7203):428–435.
- De Gassart A, et al. (2015) An inhibitor of HIV-1 protease modulates constitutive eIF2α phosphorylation to trigger a specific integrated stress response. *Proc Natl Acad Sci USA* 113(2):E117–26.
- Gant S, Casper C, Ambinder RF (2013) Insights into the broad cellular effects of nelfinavir and the HIV protease inhibitors supporting their role in cancer treatment and prevention. *Curr Opin Oncol* 25(5):495–502.
- Gills JJ, et al. (2007) Nelfinavir, a lead HIV protease inhibitor, is a broad-spectrum, anticancer agent that induces endoplasmic reticulum stress, autophagy, and apoptosis in vitro and in vivo. *Clin Cancer Res* 13(17):5183–5194.
- Hennessy M, et al. (2004) Intracellular accumulation of nelfinavir and its relationship to P-glycoprotein expression and function in HIV-infected patients. *Antivir Ther* 9(1):115–122.
- Ford J, et al. (2004) Intracellular and plasma pharmacokinetics of nelfinavir and M8 in HIV-infected patients: Relationship with P-glycoprotein expression. *Antivir Ther* 9(1):77–84.
- Martinon F, Pétrilli V, Mayor A, Tardivel A, Tschopp J (2006) Gout-associated uric acid crystals activate the NALP3 inflammasome. *Nature* 440(7081):237–241.
- LaRock CN, Cookson BT (2013) Burning down the house: Cellular actions during pyroptosis. *PLoS Pathog* 9(12):e1003793.
- Fernandes-Alnemri T, et al. (2007) The pyroptosome: A supramolecular assembly of ASC dimers mediating inflammatory cell death via caspase-1 activation. *Cell Death Differ* 14(9):1590–1604.
- Cai X, et al. (2014) Prion-like polymerization underlies signal transduction in antiviral immune defense and inflammasome activation. *Cell* 156(6):1207–1222.
- McGettrick AF, O'Neill LA (2013) NLRP3 and IL-1β in macrophages as critical regulators of metabolic diseases. *Diabetes Obes Metab* 15(Suppl 3):19–25.
- Muñoz-Planillo R, et al. (2013) K⁺ efflux is the common trigger of NLRP3 inflammasome activation by bacterial toxins and particulate matter. *Immunity* 38(6):1142–1153.
- Pétrilli V, et al. (2007) Activation of the NALP3 inflammasome is triggered by low intracellular potassium concentration. *Cell Death Differ* 14(9):1583–1589.
- Morikawa K, et al. (2014) Quantitative proteomics identifies the membrane-associated peroxidase GPx8 as a cellular substrate of the hepatitis C virus NS3-4A protease. *Hepatology* 59(2):423–433.
- Osmanagic-Myers S, Dechat T, Foisner R (2015) Lamins at the crossroads of mechanosignaling. *Genes Dev* 29(3):225–237.
- Davies BS, Fong LG, Yang SH, Coffinier C, Young SG (2009) The posttranslational processing of prelamin A and disease. *Annu Rev Genomics Hum Genet* 10:153–174.
- Guénant AC, et al. (2014) Nuclear envelope-related lipodystrophies. *Semin Cell Dev Biol* 29:148–157.
- Nolis T (2014) Exploring the pathophysiology behind the more common genetic and acquired lipodystrophies. *J Hum Genet* 59(1):16–23.
- Coffinier C, et al. (2007) HIV protease inhibitors block the zinc metalloproteinase ZMPSTE24 and lead to an accumulation of prelamin A in cells. *Proc Natl Acad Sci USA* 104(33):13432–13437.
- Perrin S, et al. (2012) HIV protease inhibitors do not cause the accumulation of prelamin A in PBMCs from patients receiving first line therapy: The ANRS EP45 “aging” study. *PLoS One* 7(12):e53035.
- Caron M, Auclair M, Sterling H, Kornprobst M, Capeau J (2003) Some HIV protease inhibitors alter lamin A/C maturation and stability, SREBP-1 nuclear localization and adipocyte differentiation. *AIDS* 17(17):2437–2444.
- Chang SY, et al. (2012) Inhibitors of protein geranylgeranyltransferase-I lead to prelamin A accumulation in cells by inhibiting ZMPSTE24. *J Lipid Res* 53(6):1176–1182.
- Leung GK, et al. (2001) Biochemical studies of Zmpste24-deficient mice. *J Biol Chem* 276(31):29051–29058.
- Goldman RD, et al. (2004) Accumulation of mutant lamin A causes progressive changes in nuclear architecture in Hutchinson-Gilford progeria syndrome. *Proc Natl Acad Sci USA* 101(24):8963–8968.
- De Vos WH, et al. (2011) Repetitive disruptions of the nuclear envelope invoke temporary loss of cellular compartmentalization in laminopathies. *Hum Mol Genet* 20(21):4175–4186.
- Cai X, Chiu YH, Chen ZJ (2014) The cGAS-cGAMP-STING pathway of cytosolic DNA sensing and signaling. *Mol Cell* 54(2):289–296.
- Schneider DS (2002) Plant immunity and film Noir: What gumshoe detectives can teach us about plant-pathogen interactions. *Cell* 109(5):537–540.
- Rathinam VA, et al. (2010) The AIM2 inflammasome is essential for host defense against cytosolic bacteria and DNA viruses. *Nat Immunol* 11(5):395–402.
- Jin T, et al. (2012) Structures of the HIN domain:DNA complexes reveal ligand binding and activation mechanisms of the AIM2 inflammasome and IFI16 receptor. *Immunity* 36(4):561–571.

47. Man SM, Karki R, Kanneganti TD (2016) AIM2 inflammasome in infection, cancer, and autoimmunity: Role in DNA sensing, inflammation, and innate immunity. *Eur J Immunol* 46(2):269–280.
48. Dombrowski Y, Koglin S, Schaubert J (2012) DNA-triggered AIM2 inflammasome activation in keratinocytes: Comment on Kopfnagel et al. *Exp Dermatol*. 2011. 20:1027–9. *Exp Dermatol* 21(6):474–475, author reply 475–476.
49. Jakobs C, Perner S, Hornung V (2015) AIM2 drives joint inflammation in a self-DNA triggered model of chronic polyarthritis. *PLoS One* 10(6):e0131702.
50. Baum R, et al. (2015) Cutting edge: AIM2 and endosomal TLRs differentially regulate arthritis and autoantibody production in DNase II-deficient mice. *J Immunol* 194(3): 873–877.
51. Paludan SR, Bowie AG (2013) Immune sensing of DNA. *Immunity* 38(5):870–880.
52. Hatch E, Hetzer M (2014) Breaching the nuclear envelope in development and disease. *Trends Cell Biol* 24(4):247–256.
53. Davidson PM, Lammerding J (2014) Broken nuclei: Lamins, nuclear mechanics, and disease. *Trends Cell Biol* 24(4):247–256.
54. de Noronha CM, et al. (2001) Dynamic disruptions in nuclear envelope architecture and integrity induced by HIV-1 Vpr. *Science* 294(5544):1105–1108.
55. Monroe KM, et al. (2014) IFI16 DNA sensor is required for death of lymphoid CD4 T cells abortively infected with HIV. *Science* 343(6169):428–432.
56. Barouch DH, et al. (2016) Rapid inflammasome activation following mucosal SIV infection of Rhesus monkeys. *Cell* 165(3):656–667.
57. Gao D, et al. (2013) Cyclic GMP-AMP synthase is an innate immune sensor of HIV and other retroviruses. *Science* 341(6148):903–906.
58. Cattin ME, et al. (2013) Heterozygous Lmna^{delK32} mice develop dilated cardiomyopathy through a combined pathomechanism of haploinsufficiency and peptide toxicity. *Hum Mol Genet* 22(15):3152–3164.
59. Sullivan T, et al. (1999) Loss of A-type lamin expression compromises nuclear envelope integrity leading to muscular dystrophy. *J Cell Biol* 147(5):913–920.
60. Osorio FG, et al. (2012) Nuclear lamina defects cause ATM-dependent NF- κ B activation and link accelerated aging to a systemic inflammatory response. *Genes Dev* 26(20):2311–2324.
61. Freund A, Orjalo AV, Desprez PY, Campisi J (2010) Inflammatory networks during cellular senescence: causes and consequences. *Trends Mol Med* 16(5):238–246.
62. Zink D, Fischer AH, Nickerson JA (2004) Nuclear structure in cancer cells. *Nat Rev Cancer* 4(9):677–687.
63. Prokocimer M, Margalit A, Gruenbaum Y (2006) The nuclear lamina and its proposed roles in tumorigenesis: Projection on the hematologic malignancies and future targeted therapy. *J Struct Biol* 155(2):351–360.
64. Denais CM, et al. (2016) Nuclear envelope rupture and repair during cancer cell migration. *Science* 352(6283):353–358.
65. Raab M, et al. (2016) ESCRT III repairs nuclear envelope ruptures during cell migration to limit DNA damage and cell death. *Science* 352(6283):359–362.
66. Man SM, et al. (2015) Critical role for the DNA sensor AIM2 in stem cell proliferation and cancer. *Cell* 162(1):45–58.
67. Wilson JE, et al. (2015) Inflammasome-independent role of AIM2 in suppressing colon tumorigenesis via DNA-PK and Akt. *Nat Med* 21(8):906–913.
68. Salminen A, Kauppinen A, Hiltunen M, Kaarniranta K (2014) Epigenetic regulation of ASC/TMS1 expression: Potential role in apoptosis and inflammasome function. *Cell Mol Life Sci* 71(10):1855–1864.
69. Shi H, et al. (2015) NLRP3 activation and mitosis are mutually exclusive events coordinated by NEK7, a new inflammasome component. *Nat Immunol* 17(3):250–8.
70. Schmid-Burgk JL, et al. (2016) A genome-wide CRISPR (Clustered Regularly Interspaced Short Palindromic Repeats) screen identifies NEK7 as an essential component of NLRP3 inflammasome activation. *J Biol Chem* 291(1):103–109.
71. Dreskin SC, Thomas GW, Dale SN, Heasley LE (2001) Isoforms of Jun kinase are differentially expressed and activated in human monocyte/macrophage (THP-1) cells. *J Immunol* 166(9):5646–5653.
72. Meunier E, et al. (2015) Guanylate-binding proteins promote activation of the AIM2 inflammasome during infection with *Francisella novicida*. *Nat Immunol* 16(5): 476–484.
73. Schoggins JW, et al. (2014) Pan-viral specificity of IFN-induced genes reveals new roles for cGAS in innate immunity. *Nature* 505(7485):691–695.
74. Meerbrey KL, et al. (2011) The pINDUCER lentiviral toolkit for inducible RNA interference in vitro and in vivo. *Proc Natl Acad Sci USA* 108(9):3665–3670.
75. Bagnis C, Bailly P, Chapel-Fernandes S (2009) Using an EGFPmeter to evaluate the lentiviral vector production: Tricks and traps. *Methods Mol Biol* 515:151–163.
76. Coffinier C, et al. (2008) A potent HIV protease inhibitor, darunavir, does not inhibit ZMPSTE24 or lead to an accumulation of farnesyl-prelamin A in cells. *J Biol Chem* 283(15):9797–9804.
77. Barrowman J, Wiley PA, Hudon-Miller SE, Hrycyna CA, Michaelis S (2012) Human ZMPSTE24 disease mutations: Residual proteolytic activity correlates with disease severity. *Hum Mol Genet* 21(18):4084–4093.
78. Sanjana NE, Shalem O, Zhang F (2014) Improved vectors and genome-wide libraries for CRISPR screening. *Nat Methods* 11(8):783–784.
79. Corrales L, et al. (2016) Antagonism of the STING pathway via activation of the AIM2 inflammasome by intracellular DNA. *J Immunol* 196(7):3191–3198.
80. Wilm M, et al. (1996) Femtomole sequencing of proteins from polyacrylamide gels by nano-electrospray mass spectrometry. *Nature* 379(6564):466–469.
81. Cox J, Mann M (2008) MaxQuant enables high peptide identification rates, individualized p.p.b.-range mass accuracies and proteome-wide protein quantification. *Nat Biotechnol* 26(12):1367–1372.
82. Cox J, et al. (2011) Andromeda: A peptide search engine integrated into the MaxQuant environment. *J Proteome Res* 10(4):1794–1805.

Supporting Information

Di Micco et al. 10.1073/pnas.1602419113

SI Materials and Methods

Cell Culture. iBMDMs from WT, caspase-1^{-/-}, NLRP3^{-/-}, AIM2^{-/-}, and ASC^{-/-} mice (a gift from D. M. Monack and P. Broz, Stanford University, Stanford, CA) and human monocytic cell line THP1 were cultured in RPMI (GIBCO) supplemented with 10% (vol/vol) FBS and 1% P/S. THP-1 cells were grown in suspension in 75-cm² flasks. MEFs, HeLa, and HEK293T cells were grown in DMEM (GIBCO) supplemented with 10% (vol/vol) FBS and 1% P/S. All cells were grown at 37 °C with 5% CO₂.

ELISA. Cytokine release was measured in supernatants from stimulated cells. For this purpose mouse IL-1β and human IL-1β ELISA kits (eBioscience) were used according to the manufacturer's instructions.

Chemicals and Antibodies. Nelfinavir mesylate (CAS 159989–65-8) was from Axon Medchem. Amprenavir, Ritonavir, Atazanavir, Lopinavir, and Saquinavir were obtained from the NIH AIDS Reagent Program. Ultra-pure LPS from *Escherichia coli* was from Invivogen. ATP, NG, poly(dA:dT), PMA, Efavirenz, Thapsigargin, Brefeldin, *N*-acetyl-cysteine, the protonophore CCCP, and etoposide were from Sigma. Tipranavir was from Santa Cruz Biotechnology. MSU crystals were prepared as previously described (24). Z-Vad-FMK was from Bachem. Lipofectamine 2000 was from Invitrogen. Tunicamycin was from Enzo Life Sciences. GGTI was from R&D Systems. The anti-mouse IL-1β antibody was from R&D System. The anti-mouse caspase-1 p20, anti-mouse ASC antibody, anti-NLRP3, anti-human caspase-1, and anti-human tubulin were from Adipogen. The anti-human ASC antibody was from MBL. The anti-mouse ATF4, anti-mouse lamin B1, anti-human lamin A/C, anti-human prelamin A, and anti-dsDNA antibodies were from Santa Cruz. The anti-human γH2AX antibody was from Millipore. The anti-human p-CHK1 antibody was from Cell Signaling. Anti-Flag antibody was from GenScript. Flow cytometry antibodies anti-mouse IL-6-APC, anti-mouse TNF-PE, anti-mouse LY6G-PE, anti-mouse LY6C-FITC, and anti-mouse CD11b-APC were from eBioscience.

Generation of shRNA Clones. Lentiviruses for shRNA were produced by cotransfecting HEK293T cells with the following different shRNA-containing plasmids targeting AIM2 or ASC (pLKO.1 plasmids: shAIM2—5'-CCA ACT GGT CTA AGC ATT-3'; 5'-CCC GCT GAA CAT TAT CAG AAA-3'; 5'-AGC CAC TAA GTC AAG CTG AAA-3'; 5'-CTG GAG TTC ATA GCA CCA TAA-3'; 5'-GCC ACT AAG TCA AGC TGA AAT-3'; shASC—5'-GCC CAC CAA CCC AAG CAA GAT-3') plus a lentiviral packaging system (pMD2 VSV and pCMV DR8.91). Cells were transfected using TransIT 2020 transfection reagent (MIRUS). Supernatant was collected at 72 h posttransfection and filtered with a 0.45-mm filter to clear cell debris. THP1 cells were resuspended in the virus-containing supernatant for infection. After 48 h the medium was changed with complete RPMI plus 4 mg/mL of puromycin (Enzo Life Sciences) for generation of stable cell lines. Cells were subjected to selection for 7 d, and expression levels of AIM2 or ASC were checked by Western blot.

Generation of CRISPR/Cas9 Clones. CRISPR sequences targeting exon 3 of human STING and exon 1 of ZMPSTE24 were designed using the online-available CRISPR design tool developed by the F. Zhang laboratory. The seed sequences preceding the protospacer adjacent motif (PAM) are the following: STING oligo 1—5'-CACCGAGAGCACACTCTCCGGTACC-3'; STING oligo

2—5'-AAACGGTACCGGAGAGTGTGCTCTC-3'; ZMPSTE24 oligo 1—5'-CACCGCCGG CCGAGAAGCGTATCT-3'; and ZMPSTE24 oligo 2—5'-AAACAAGATACGTTCTCGGCCGGC-3'. We used a sequence targeting luciferase as nonrelevant single-guide RNA (sgRNA) (CTTCGAAATGTCCGTTCCGGT): luciferase oligo 1—5'-CACCGCTTCGAAATGTCCGTTCCGGT-3'; and luciferase oligo 2—5'-AAACACCGAACGGACATTTTCGAAGC-3'. Nucleotides in italics show the overhangs necessary for incorporation into the restriction enzymatic site BbsI of LentiCRISPR-v2 vector expressing Cas9 and sgRNA (Adgene #52961) (78). Lentiviruses were produced in 293T cells as previously described (75). HeLa cells were infected with lentiCRISPRv2 viruses targeting STING, Zmpste24, or luciferase. Positive cells were selected with 2 μg/mL puromycin for 15 d. STING expression was assessed by immunoblotting. To obtain full KO cell lines, population was cloned by limit dilution and tested again by immunoblotting.

RNA Extraction and RT-PCR of IFN-Responsive Genes. Total RNA from cells was extracted using PeqGOLD TriFast (PeqLab) and reverse-transcribed into cDNA with a High Capacity cDNA Reverse Transcription kit (Applied Biosystems). Quantitative RT-PCR was done with Roche SYBR green fluorescent reagent and Roche Lightcycler480 Real Time PCR System. mRNA was quantified using the comparative threshold cycle method with β-actin as control. Primers used were the following: Actin-Fwd—5'-TACCACCATGTACCCAGGCA-3'; Actin-Rev—5'-CTCAGGAGAGCAATGATCTTGAT-3'; ISG15-Fwd—5'-GGTGACAAATGCGACGAA-3'; ISG15-Rev—5'-TGCTGCGGCCTTGTTAT-3'; Cxcl10-Fwd—5'-AAGTGCTGCCGTCATTCTCT-3'; Cxcl10-Rev—5'-CCTATGGCCCTCATTCTCAC-3'; Ifnb-Fwd—5'-GGAGATGACGGAGAAGATGC-3'; Ifnb-Rev—5'-CCCAGTGCTGGAGAAATTGT-3'; Isg15-Fwd—5'-AGCGGACAAGTCACGAAGAC-3'; and Isg15-Rev—5'-TGGGGCTTAGGCCATACTC-3'. BMDMs and MEFs were stimulated with NFR or poly(dA:dT) for 15 h in the presence of 10 μM Z-VAD-FMK to limit pyroptosis inflammasome and subsequent down-regulation of type I IFN responses (79).

Membrane Potential Measurement. Mitochondrial membrane potential was determined using the Mitochondrial Permeability Detection kit (BIOMOL International). iBMDMs were primed with LPS and stimulated with ATP, MSU, CCCP, or NFR. After stimulation, the cells were incubated with JC-1 (5,5,6,6'-tetrachloro-1,1',3,3'-tetraethylbenzimidazolocarbo-cyanine iodide) for 20 min at 37 °C. JC-1 is a mitochondrial dye that accumulates in the matrix of intact mitochondria and forms red fluorescent aggregates with a fluorescence emission of ~590 nm. When membrane potential decreases, JC-1 dissociates into green fluorescent monomers with a fluorescence emission of ~529 nm. Consequently, mitochondrial depolarization was measured by a decrease in the red/green fluorescence intensity ratio. The fluorescence was detected by a Gemini XPS Fluorescent Microplate Reader.

Slice-SILAC, Protein Separation, and MS. The Slice-SILAC screen was performed in HeLa cells in the presence or absence of 10 μM NFR for 6 h. Cells were lysed in a buffer containing 4% (wt/vol) SDS, 0.1 M DTT, and 100 mM Tris-Cl, pH 7.5, followed by sonication for three cycles of 5 s on ice and centrifugation for 10 min at 11,000 × g to pellet nuclei and cellular debris. Protein concentrations in supernatants were determined using the Bradford protein assay (Bio-Rad) and verified by densitometry

scanning of whole lanes of SDS/PAGE gels after Coomassie staining. For protein separation, lysates were mixed at a quantitative ratio of 1:1. A total of 20 μ g of protein from mixed lysates was migrated on a precast 8–16% Novex NuPAGE SDS Mini Gel (Invitrogen). Entire lanes were cut into 48 identical gel slices. In-gel proteolytic cleavage with sequencing grade trypsin (Promega) was performed as described (80). The supernatant from the digestion was concentrated by evaporation and redissolved in 30 μ L 0.1% formic acid in 2% acetonitrile for liquid chromatography coupled with tandem mass spectrometry. Samples were analyzed on a hybrid linear trap LTQ-Orbitrap Velos mass spectrometer (Thermo Fisher) interfaced via a nanospray source to a Dionex RSLC 3000 nanoHPLC system (Dionex). Peptides were separated on a reversed-phase Acclaim PepMap nanocolumn (75- μ m inner diameter \times 25 cm, 2- μ m particle size, 100- Å pore size; Dionex) with a 5–85% acetonitrile gradient in 0.1% formic acid (total time 90 min). Full MS survey scans were performed at 60,000 resolution. In data-dependent acquisition controlled by Xcalibur 2.0.7 software (Thermo Fisher), the 20 most intense multiply charged precursor ions detected in the full MS survey scan were selected for collision-induced dissociation (CID) fragmentation in the ion trap and then excluded from further selection during 120 s.

MS Data Analysis. MS data were analyzed and quantified using MaxQuant version 1.4.1.2 (81), using the Andromeda search engine for identification (82). Database searches were performed on the human subset of the UniProtKB/SWISSPROT database,

version 2014_05 containing 85,919 sequences and supplemented with common contaminants (81). Search parameters were trypsin specificity, two possible missed cleavages, and mass error tolerances of 7 ppm for the precursor and 0.5 Da for CID tandem mass spectra. The iodoacetamide derivative of cysteine was specified as a fixed modification, and oxidation of methionine and protein N-terminal acetylation were specified as variable modifications. Protein identifications were filtered at a 1% false discovery rate established against a reversed database, according to default MaxQuant parameters. A minimum of one unique peptide was necessary to discriminate sequences that shared peptides. Sets of protein sequences that could not be discriminated based on identified peptides were listed together as protein groups. MaxQuant analysis used an experimental design file in which every dataset corresponding to a gel slice was quantified separately as a distinct experiment and numbered as the gel slice with which it corresponded. Results from MaxQuant were filtered and processed further with custom-built software tools. The first was a Perl script that filtered the main MaxQuant result to identify proteins present in at least two distinct gel slices with different SILAC ratios and a certain number of evidence counts, as described in *Results*. Next, the evidence counts and normalized SILAC ratios for these selected proteins were visualized as a function of the gel slice with an R script. The size and color of the circles were scaled to represent the number of evidences found and the \log_2 of the normalized SILAC ratios, respectively.

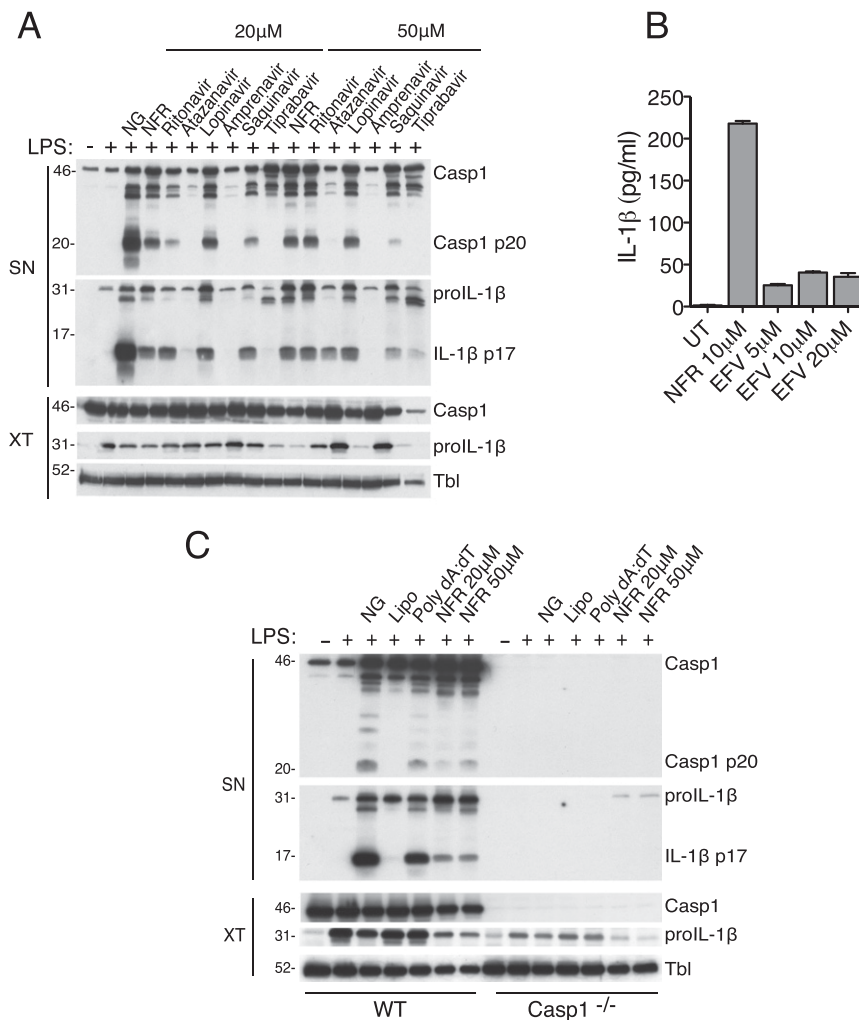


Fig. S1. HIV-PIs activation of caspase-1. (A) LPS-primed BMDMs treated with NG and two concentrations (20 μ M, 50 μ M) of NFR or a panel of HIV-PIs was analyzed for caspase-1 and IL-1 β maturation by immunoblotting. SN: supernatants; XT: cell extracts. Tubulin (Tbl) was used as a loading control. Data are representative of three independent experiments. (B) BMDMs were treated with NFR or increasing doses of the nonnucleoside reverse transcriptase inhibitor Efavirenz. IL-1 β release was measured by ELISA. Data are representative of two independent experiments. (C) Immunoblot analysis of caspase-1 and IL-1 β maturation in caspase-1/11-deficient BMDMs and control (WT) primed with LPS as indicated and treated with NG, Lipo, poly(dA:dT), or NFR.

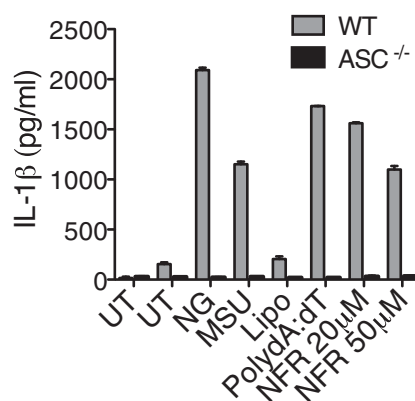


Fig. S2. ASC is required for NFR-mediated maturation of IL-1 β . ASC-deficient and control (WT) BMDMs primed with LPS as indicated were treated with NG, MSU, Lipo, poly(dA:dT), or NFR. IL-1 β release was measured by ELISA. Data are representative of three independent experiments.

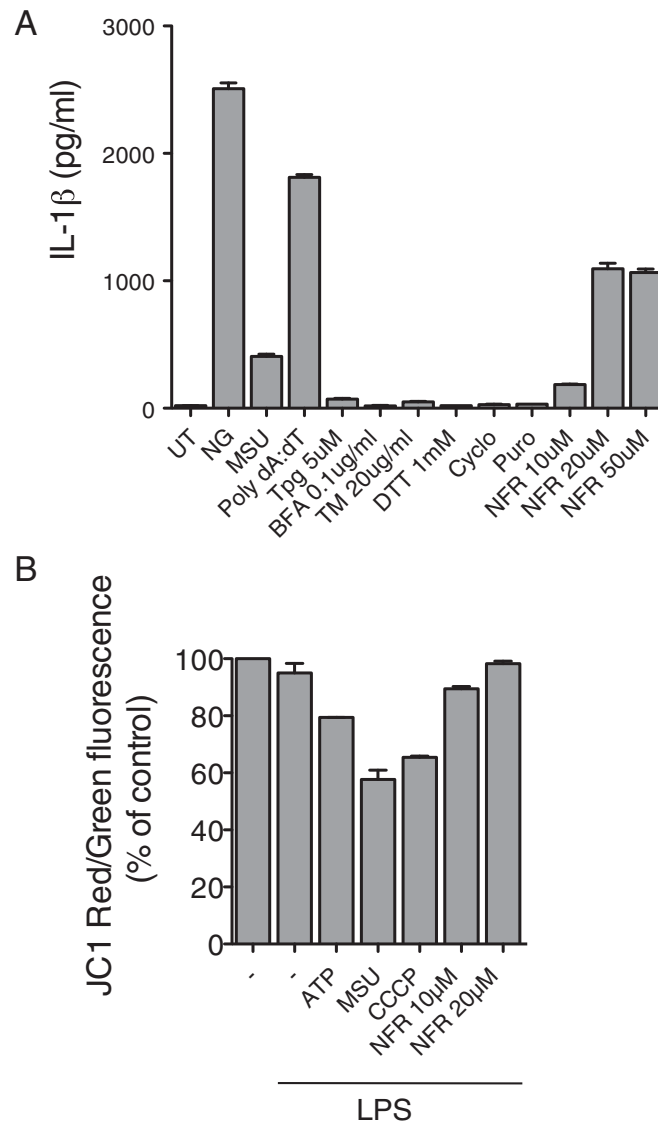


Fig. S3. NFR does not affect mitochondrial membrane potential and drives a robust inflammasome response. (A) BMDMs primed with LPS and treated with NG, MSU, poly(dA:dT). ER-stress inducers: brefeldin A (BFA), thapsigargin (Tpg), tunicamycin (TM), and DTT. Protein translation inhibitors: cycloheximide (Cyclo), puromycin (Puro), or NFR. IL-1 β release was measured by ELISA. UT, untreated. (B) The mitochondrial membrane potential was measured with JC-1 dye in BMDMs primed with LPS and treated with extracellular ATP, MSU, CCCP, or NFR. Data are representative of three independent experiments.

